



**HAL**  
open science

## **A silicon nanomembrane platform for the visualization of immune cell trafficking across the human blood–brain barrier under flow**

Adrien Mossu, Maria Rosito, Tejas Khire, Hung Li Chung, Hideaki Nishihara, Isabelle Gruber, Emma Luke, Lucie Dehouck, Federica Sallusto, Fabien Gosselet, et al.

### ► To cite this version:

Adrien Mossu, Maria Rosito, Tejas Khire, Hung Li Chung, Hideaki Nishihara, et al.. A silicon nanomembrane platform for the visualization of immune cell trafficking across the human blood–brain barrier under flow. *Journal of Cerebral Blood Flow and Metabolism*, 2018, 39 (3), pp.395-410. 10.1177/0271678X18820584 . hal-02505603

**HAL Id: hal-02505603**

**<https://univ-artois.hal.science/hal-02505603v1>**

Submitted on 10 Jan 2022


**HAL** is a multi-disciplinary open access archive for the deposit and dissemination of scientific research documents, whether they are published or not. The documents may come from teaching and research institutions in France or abroad, or from public or private research centers.

L'archive ouverte pluridisciplinaire **HAL**, est destinée au dépôt et à la diffusion de documents scientifiques de niveau recherche, publiés ou non, émanant des établissements d'enseignement et de recherche français ou étrangers, des laboratoires publics ou privés.



Distributed under a Creative Commons Attribution - NonCommercial 4.0 International License

# A silicon nanomembrane platform for the visualization of immune cell trafficking across the human blood–brain barrier under flow

Adrien Mossu<sup>1,\*</sup> , Maria Rosito<sup>1,\*</sup>, Tejas Khire<sup>2</sup>, Hung Li Chung<sup>2</sup>, Hideaki Nishihara<sup>1</sup>, Isabelle Gruber<sup>1</sup>, Emma Luke<sup>2</sup>, Lucie Dehouck<sup>3</sup>, Federica Sallusto<sup>4,5</sup>, Fabien Gosselet<sup>3</sup>, James L McGrath<sup>2</sup> and Britta Engelhardt<sup>1</sup>

## Abstract

Here we report on the development of a breakthrough *microfluidic* human *in vitro* cerebrovascular barrier (CVB) model featuring stem cell-derived brain-like endothelial cells (BLECs) and nanoporous silicon nitride (NPN) membranes ( $\mu$ SiM-CVB). The nanoscale thinness of NPN membranes combined with their high permeability and optical transparency makes them an ideal scaffold for the assembly of an *in vitro* microfluidic model of the blood–brain barrier (BBB) featuring cellular elements of the neurovascular unit (NVU). Dual-chamber devices divided by NPN membranes yield tight barrier properties in BLECs and allow an abluminal pericyte-co-culture to be replaced with pericyte-conditioned media. With the benefit of physiological flow and superior imaging quality, the  $\mu$ SiM-CVB platform captures each phase of the multi-step T-cell migration across the BBB in live cell imaging. The small volume of  $<100\ \mu\text{L}$  of the  $\mu$ SiM-CVB will enable *in vitro* investigations of rare patient-derived immune cells with the human BBB. The  $\mu$ SiM-CVB is a breakthrough *in vitro* human BBB model to enable live and high-quality imaging of human immune cell interactions with the BBB under physiological flow. We expect it to become a valuable new tool for the study of cerebrovascular pathologies ranging from neuroinflammation to metastatic cancer.

## Keywords

Blood–brain barrier, microfluidics, nanoporous silicon nitride membrane, two-compartmental flow chamber, T-cell migration

Received 15 August 2018; Revised 21 November 2018; Accepted 23 November 2018

## Introduction

The endothelial blood–brain barrier (BBB) in central nervous system (CNS) parenchymal microvessels protects the CNS from the constantly changing milieu in the blood stream. Low pinocytotic activity, complex, and molecularly distinct tight junctions combined with expression of specific transporters and enzymes make BBB endothelial cells (ECs) biochemically unique.<sup>1</sup> Importantly, development and maintenance of BBB characteristic in CNS microvascular endothelium is not an intrinsic characteristic but rather relies on the continuous cross-talk with cellular and acellular components of the neurovascular unit.<sup>1</sup> In addition to strictly controlling the movement of molecules across

<sup>1</sup>Theodor Kocher Institute, University of Bern, Bern, Switzerland

<sup>2</sup>Department of Biomedical Engineering, University of Rochester, Rochester, NY, USA

<sup>3</sup>Blood Brain Barrier Laboratory, University of Artois, Lens, France

<sup>4</sup>Institute for Research in Biomedicine, Università della Svizzera Italiana, Bellinzona, Switzerland

<sup>5</sup>Institute for Microbiology, ETH Zurich, Zurich, Switzerland

\*These authors contributed equally to this article.

## Corresponding authors:

Britta Engelhardt, Theodor Kocher Institute, University of Bern, Bern 3012, Switzerland.

Email: [bengel@tki.unibe.ch](mailto:bengel@tki.unibe.ch)

James L McGrath, University of Rochester, Rochester, NY 14627, USA.

Email: [jmcgrath@bme.rochester.edu](mailto:jmcgrath@bme.rochester.edu)

its interfaces, the BBB also rules the entry of immune cells and immune mediators into the immune-privileged CNS.<sup>2</sup> While under physiological conditions immune cell entry into the CNS is very low, in CNS inflammatory diseases such as multiple sclerosis (MS), BBB function is impaired and high numbers of immune cells infiltrate the CNS, where they cause inflammation and demyelination.<sup>3</sup> Therapeutic inhibition of immune cell entry into the CNS has proven beneficial for the treatment of MS.<sup>4</sup> Unfortunately, these therapies come with the rare, but severe side effect of progressive multifocal leukoencephalopathy (PML), which is caused by infection of human oligodendrocytes with the JC virus and can thus not be modeled in animals. Furthermore, a number of anti-inflammatory treatments that were highly effective in animal models for MS, have failed in MS trials,<sup>5</sup> underscoring that the autoimmune pathogenesis underlying MS including BBB dysfunction and immune cell entry into the CNS cannot be modeled in their entire complexity in available animal models. Therefore, there is an unmet need for detailed functional studies employing human disease-relevant tissues and cells. This includes the necessity for human models of the BBB allowing the study of its function and the migration by disease-relevant immune cell subsets across the cellular barrier as a critical step in MS pathogenesis.

Most well-characterized BBB culture models are based on primary brain ECs or brain EC lines from animal origin (bovine, porcine, and murine).<sup>6–8</sup> Although elegant human *in vitro* BBB models employing primary human brain ECs have been established,<sup>9</sup> their availabilities are limited to few laboratories with privileged access to human brain tissue. Thus, human brain EC lines like the hCMEC/D3 have been established and widely used as *in vitro* models of the human BBB.<sup>10,11</sup> Although hCMEC/D3 retain morphological and functional characteristics of human brain endothelium, they fail to establish barrier characteristics resembling their tightness observed in BBB *in vivo*.<sup>12</sup> This limits the suitability of hCMEC/D3 for pharmacological, toxicological, and functional assays on the human BBB with *in vivo* predictability.

Recently, stem cell sources have demonstrated substantial advantage over other brain ECs sources for BBB modeling given their human origin, stability, scalability, self-renewal, and potential to generate syngeneic cellular components of the neurovascular unit.<sup>13,14</sup> While inducible pluripotent stem cell-derived *in vitro* BBB models establish very tight barrier properties, their immune phenotype has not been well established. We have recently employed cord blood CD34<sup>+</sup> hematopoietic stem cells to differentiate ECs.<sup>15</sup> By co-culturing CD34<sup>+</sup>-derived ECs with bovine pericytes, we were able to differentiate those ECs into brain-like endothelial cells (BLECs) providing a

valuable *in vitro* model for the human BBB.<sup>15</sup> Growing BLECs on conventional cell culture filter inserts in co-culture with pericytes, we and others used both small molecule diffusion and transendothelial electrical resistance to establish that BLECs form tight barriers, show robust expression of BBB signature molecules<sup>15,16</sup> and express adhesion molecules supporting T-cell trafficking across the BBB.<sup>17</sup> In combination with their large-scale availability, BLECs are therefore the ideal culture platform to study the interaction of human immune cells with the human BBB *in vitro*.<sup>17</sup>

Live cell imaging on glass coverslips has been used historically as the means of monitoring immune cell migration across endothelial monolayers *in vitro* under static and flow conditions.<sup>18–21</sup> As glass coverslips are impermeable, they are not suited for establishing *in vitro* BBB models that rely on the cross-talk between brain microvascular ECs in a luminal compartment and CNS-derived factors in an abluminal compartment.<sup>22,23</sup> On the other hand, the imaging qualities of permeable polymer track-etched (TE) membranes used in filter inserts are too poor to study immune cell interactions with the BBB *in vitro* by live cell imaging. Several studies have also demonstrated that physiological shear forces are key to the multi-step process of T-cells diapedesis.<sup>8,24,25</sup> Thus, the ideal platform for the study of dynamic T-cell interactions with the BBB is a membrane-based flow microfluidic system with glass-like imaging quality.

Here, we report on the development of a novel *in vitro* platform, the  $\mu$ SiM-CVB, for the study of the interaction of human T cells with human *in vitro* models of the BBB. The enabling component of this platform is ultrathin nanoporous silicon nitride (NPN), a 50 nm thick “nanomembrane” with a high density ( $10^{10}$  cm<sup>-2</sup>; 20% porosity) of  $\sim$ 40 nm pores.<sup>26,27</sup> The thinness and high porosity of NPN result in a luminal/abluminal divider with extraordinary small molecule permeability,<sup>27,28</sup> and the sub-optical pore sizes of NPN provide outstanding imaging characteristics. We establish that CD34<sup>+</sup> stem cell-derived ECs differentiate into BLECs when cultured on NPN with pericyte-conditioned medium supplied basolaterally, eliminating the confounding effects of subluminal cell cultures on imaging. Finally, we demonstrate the utility of the  $\mu$ SiM-CVB by capturing each phase of multi-step T-cell migration across the BBB using live cell imaging under physiological flow.

## Material and methods

### Device fabrication

The enabling feature of our engineered devices used in this study is NPN membranes, also referred to as

nanomembranes. The details of the fabrication of these membranes are provided elsewhere<sup>26</sup> and are commercially available at SiMPore Inc., West Henrietta, NY. The overall dimension of the NPN membrane is  $5.4 \times 5.4 \times 0.3 \text{ mm}^3$  and the permeable freestanding “window” of the chip is  $2 \text{ mm} \times 0.7 \text{ mm} \times 0.05 \text{ mm}$  (50 nm) and have an average pore diameter of 50 nm.

The microfluidic device used for static and dynamic assays consists of two compartments: apical and basal, separated by the permeable membrane chip in between. The apical and basal fluidic compartments or channels are composed of transparent 300  $\mu\text{m}$  silicone gaskets (Specialty Silicone Fabricators, CA). The different layers of the static and flow devices are shown in Figures 3 and 4, respectively. The channels and the silicon chip are irreversibly bonded to each other by exposing them to UV-Ozone for 10–15 min followed with curing at 70°C for 2 h. The fluidic access ports for these devices are provided by a thick slab of polydimethyl siloxane (PDMS) (Sylgard 184, Dow Corning). Flow devices have four access ports (~1 mm holes punched in the PDMS blocks): two for the apical chamber and two for the basal chamber, while “Transwell® mimetics” only have access ports for the basal chamber. Upper PDMS blocks also have wider punched holes that act as media reservoirs to support cell culture in both types of devices and are bonded to the remaining device using same UV-ozone treatment.

### CD34<sup>+</sup> cell-derived in vitro BBB model

CD34<sup>+</sup> cells were isolated from human umbilical cord blood (UCB) according to a protocol previously reported.<sup>29</sup> The isolation of CD34<sup>+</sup> cells required the collection of human UCB from infants. According to the articles L.1243-3 and R.1234-49 of the French legislation regarding the collection, the use for Research of tissues and cells coming from human body and its derivatives, organs and blood, UCB collection was approved by the Hospital ethical committee (Béthune Maternity Hospital, Béthune, France). The protocol regarding the use of human tissues and cells was authorized by the French Ministry of Higher Education and Research (CODECOH Number DC2011-1321). CD34<sup>+</sup> cells isolated from the UCB were differentiated in ECM basal medium (ScienCell) supplemented with 20% (v/v) fetal bovine serum (FBS; Life Technologies), and 50 ng/mL of VEGF<sub>165</sub> (PeproTech Inc.), on 1% (w/v) gelatin-coated 24-well plates ( $2 \times 10^5$  cells/well). After 15–20 days, ECs are seen in the culture dish. For each experiment, the cells were expanded in 0.2% (w/v) gelatin-coated 100 mm Petri dishes (Corning) in ECM basal medium supplemented with 5% FBS, 1% endothelial cell growth supplement (ECGS; ScienCell), and 50  $\mu\text{g}/\text{mL}$  gentamycin (Biochrom AG).

Induction of BBB-like characteristics in CD34<sup>+</sup>-derived ECs was achieved by co-culture with bovine pericytes as described before<sup>15</sup> and elaborated on in Supplementary Methods.

### Endothelial permeability (Pe) and stimulation

Endothelial permeability was investigated by measuring the clearance of Lucifer yellow (LY; 20 nM; Life technologies) across the BLECs monolayer exactly as described<sup>15,30–32</sup> and elaborated in Supplementary Methods. Pro-inflammatory conditions were induced by stimulation with 10 ng/mL human recombinant tumor necrosis factor- $\alpha$  (TNF- $\alpha$ , 210-TA, R&D Systems, Inc.) for 16 to 20 h prior to the experiments.

### Immunofluorescence stainings of BLECs

*For staining in the Transwell® filter inserts*, BLECs were fixed in 1% (w/v) formaldehyde and permeabilized in Triton X-100 (0.1% (w/v) at room temperature (RT). Then filter membranes were blocked for 30 min with skimmed milk 5% (w/v) in PBS. BLEC monolayers were incubated for 1 h at RT with antibodies against anti-zonula occludens-1 (ZO-1) or VE-Cadherin. For claudin-5 staining, BLECs were fixed in methanol at –20°C for 30 s prior to the staining procedure. For ICAM-1, ICAM-2, and VCAM-1, live BLECs were incubated with 10  $\mu\text{g}/\text{mL}$  of the respective antibody for 20 min at 37°C in the culture medium, fixed and permeabilized as described.<sup>17</sup> Secondary antibodies were incubated for 30 min at RT. For F-actin staining, after Triton permeabilization, cells were incubated with rhodamine-labeled phalloidin for 1 h at RT. Nuclei were stained with DAPI at 1  $\mu\text{g}/\text{mL}$ .

*For BLECs staining on NPN membranes*, live cells were incubated with 10  $\mu\text{g}/\text{mL}$  of anti-ICAM-1, ICAM-2, or VCAM-1 antibody for 20 min at 37°C in the culture medium. Then, BLECs were fixed and permeabilized according to the Transwell® inserts protocol. For the claudin-5 and F-actin staining, the same protocol as for BLECs staining on Transwell® filters was applied. After PBS washes, secondary antibodies were incubated for 30 min at RT. A detailed protocol is included in Supplementary Methods.

### Human peripheral blood T cells

Human CD4<sup>+</sup>CD45RO<sup>+</sup> T helper 1 (Th1) cells were obtained by fluorescence activated cell sorting from the peripheral blood of healthy donors according to their specific expression pattern of chemokine receptors (CXCR3<sup>+</sup>, CCR4<sup>neg</sup> CCR6<sup>neg</sup>) exactly as previously described.<sup>33,34</sup> Th1 cells were cultured in the presence of interleukin-2 (IL-2, 500 U/mL) for a total of 20 days.

At the day of the experiment, dead cells were removed by a Ficoll gradient (780 g, 20 min, 20°C), and Th1 cells were resuspended in migration assay medium (DMEM w/o phenol red, Hepes 25 mM, fetal bovine serum 5%, L-glutamine 4 mM) at  $1 \times 10^6$  cells/mL.

### *In vitro live cell imaging*

BLECs were grown to confluency in ECM basal medium supplemented with 5% FBS, 1% ECGS and 50  $\mu$ g/mL gentamycin for six days as described before and stimulated or not 16 h to 20 h prior to the assay with TNF- $\alpha$  at 10 ng/mL (R&D System, 210-TA). Flow was applied by connecting the outlet tubing to a syringe automatically drawn up by a precision pump (Harvard Apparatus, Holliston, MA, USA). The flow rate was calculated as described in Coisne et al.<sup>18</sup> To allow for the accumulation of sufficient Th1 cells on the BLECs monolayer, Th1 cells were first infused with a flow rate of 0.1 dyne/cm<sup>2</sup> for 4 min (accumulation phase). After the accumulation phase, the tap is switched to infuse migration assay medium only and the flow rate was increased to 1.5 dyne/cm<sup>2</sup> for 30 min (shear phase). T-cell interaction with the BLECs was recorded for 30 min in time lapse mode (1 picture/5 s) using the microscopic equipment that has been described in depth before<sup>18</sup> with the ZEN blue software. Video editing was performed with the software “Adobe After Effect” allowing to export the image sequences as videos running at 30 frames/s as well as to edit the videos to show the different T-cell behavior with the BLECs. Fiji software was used to classify the T-cell behavioral categories observed on the BLECs under physiological flow (diapedesis, crawling, probing, and detaching).

### *Statistical analysis*

Data are shown as the mean  $\pm$  SD. Statistical significance was assessed by Student’s t-test or one-way ANOVA followed by Dunett’s post hoc test. For multiple comparison, p-values are indicated in the corresponding figures (\*p < 0.05, \*\*p < 0.01, \*\*\*p < 0.001, \*\*\*\*p < 0.0001). Statistical analyses comprising calculation of degrees of freedom were done using GraphPad Prism 6 software (Graphpad software, La Jolla, CA, USA).

## **Results**

### *Commercial supports are not suitable for live cell imaging of the human in vitro BBB model under physiological flow*

We have previously developed a custom-made flow chamber that allowed us to observe the interaction of

immune cells with an in vitro model of the mouse BBB established from primary mouse brain microvascular endothelial cells (pMBMECs) by live cell imaging.<sup>18</sup> More recently, we adapted this flow chamber to allow the insertion of commercially available filter membranes.<sup>35</sup> In addition to a significant reduction in imaging quality, we found that the commercial TE membranes could not support the formation of BLEC monolayers or that they immediately resulted in the detachment of the monolayer with the onset of flow (Supplementary videos 1–4). We found similar negative results with 6 commercially available polymer filters (Supplementary Table 1) even with the addition of Matrigel<sup>TM</sup>, laminins, collagens or fibronectin coatings.

A review of experimental microfluidic culture devices described in the literature suggests that these would not provide ready solutions to our needs. Most generally, these systems are not amenable to live cell observations of T cell/BLEC interactions due to the lack of membrane transparency,<sup>36,37</sup> and/or due to the fact that the EC interface is grown vertically<sup>38</sup> or on the luminal surface of tubings.<sup>39–41</sup> Moreover, some of these systems employ large amounts of fluid volume to maintain flow over time,<sup>36,37,42</sup> which would limit our ability to study the interaction of rare patient-derived T-cell subsets with BLECs. We concluded that both a novel membrane and microfluidic device were needed for live cell imaging of dynamic human T-cell/BBB interactions in vitro.

### *CD34<sup>+</sup>-derived ECs adhere and grow on NPN membranes*

We established that CD34<sup>+</sup>-derived ECs readily adhered to and built a confluent monolayer on Matrigel<sup>TM</sup>-coated NPN under static conditions and that NPN provided glass-like clarity of monolayers in phase contrast microscopy (Figure 1). NPN is a recently developed ultrathin silicon membrane technology<sup>26</sup> and the third generation of ultrathin porous “nanomembranes” developed using silicon manufacturing techniques.<sup>28,43</sup> NPN membranes are 50 nm thick with  $\sim$ 20% porosity and a narrow distribution of pores centered around 40 nm. NPN is far more mechanically and chemically robust than our original porous nanocrystalline silicon membranes,<sup>26</sup> and unlike microporous SiO<sub>2</sub> membranes,<sup>43,44</sup> the nanoscale pores of NPN are invisible to light microscopy. Importantly, we have found that NPN supports vascular EC adhesion under physiological shear stress, while microporous SiO<sub>2</sub> nanomembranes do not (Supplemental Figure S1), perhaps related to the fact that micron-scale pores disrupt the normal architecture of basement membranes.<sup>45</sup>



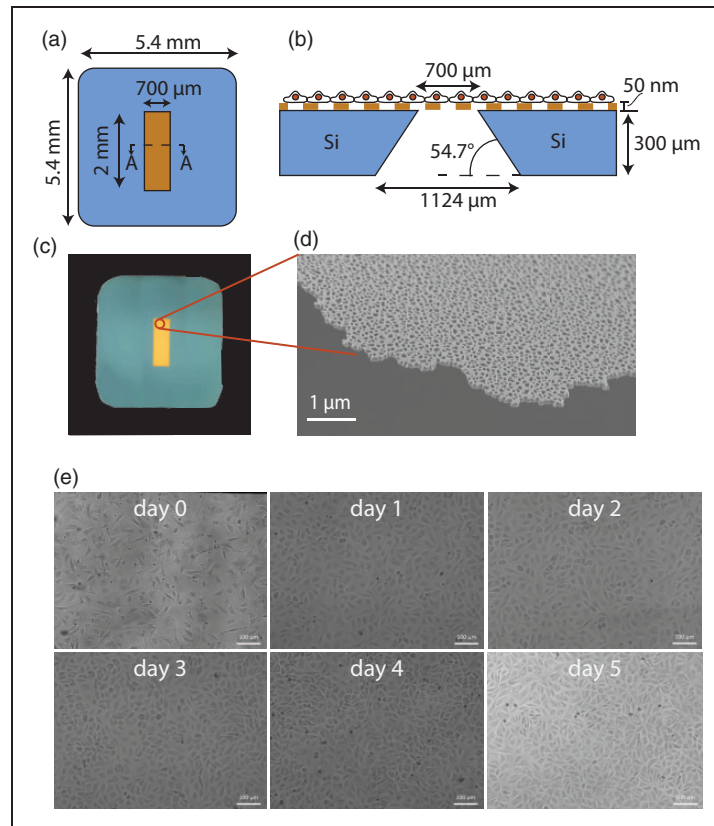


**Figure 1.** CD34<sup>+</sup>-derived ECs grow to confluent monolayer on the nanoporous silicon nitride membrane (NPN). (a) Schematic of the nanoporous silicon nitride membrane used for the cell culture experiments. The free-standing membrane region is a 2 mm × 0.7 mm window in the center of a 5.4 mm × 5.4 mm membrane “chip.” (b) The cross-sectional (a–a) schematic of the membrane. The bulk substrate consists of 300 μm of crystalline silicon, which is etched at the center to remove the bulk leaving a free standing 50-nm thin silicon nitride membrane. The manufacturing of these membranes was described before.<sup>26</sup> (c) Optical micrograph of the membrane chip. (d) Scanning electron micrograph demonstrating the ultrathin nature and porous structure of NPN (>20% porosity in this example). (e) Phase contrast pictures of CD34<sup>+</sup>-derived ECs adhering and growing to confluent monolayer on the NPN membranes from day 0 until day 5 after plating. The CD34<sup>+</sup> ECs adhere on the NPN membrane after 1 to 2 h and start to grow to form a confluent monolayer between 1 and 2 days of culture. Cellular density increases until day 5. Scale bar, 100 μm.

*Pericyte co-culture can be replaced by pericyte-conditioned medium to induce BBB characteristics in CD34<sup>+</sup>-derived ECs.* Co-culture of CD34<sup>+</sup>-derived ECs with pericytes is essential for induction of BBB characteristics as complex tight junctions and expression of transporters.<sup>15</sup> However, shadows from out-of-focus pericytes in the basal chamber impair imaging of T-cell/endothelial interactions in a co-culture system. Thus, to improve the imaging quality at the level of the endothelial layer, we asked if the pericyte-co-culture could be simply replaced with conditioned medium from the pericyte cultures. To this end, we co-cultured CD34<sup>+</sup>-derived ECs with or without pericytes in the original Transwell<sup>®</sup> filter co-culture setup for five days as positive and negative control, respectively. In parallel, CD34<sup>+</sup>-derived ECs plated on additional Matrigel-coated Transwell<sup>®</sup> filter inserts were co-incubated

with pericyte-conditioned medium (PCM) from the abluminal (lower compartment) or luminal (upper compartment) side (Figure 2(a) and (b)) and subsequently replaced on a daily basis by alternating between 24 h and 48 h conditioned medium. In order to obtain the PCM, 2.25 × 10<sup>4</sup>/well pericytes were seeded into 24-well Costar plates one day prior to seeding the CD34<sup>+</sup>-derived ECs. After the adhesion of the CD34<sup>+</sup>-derived ECs on the Matrigel-coated Transwell<sup>®</sup> filter inserts, the 24 h PCM was collected from the pericyte cultures and administered to the luminal or abluminal side of the CD34<sup>+</sup>-derived ECs (Figure 2(a) and (b)) and subsequently replaced on a daily basis by alternating between 24 h and 48 h PCM to ensure an optimal concentration of the pericyte-derived factors (Figure 2(b)). After five days of culturing the CD34<sup>+</sup>-derived ECs under the different conditions, their barrier characteristics were compared

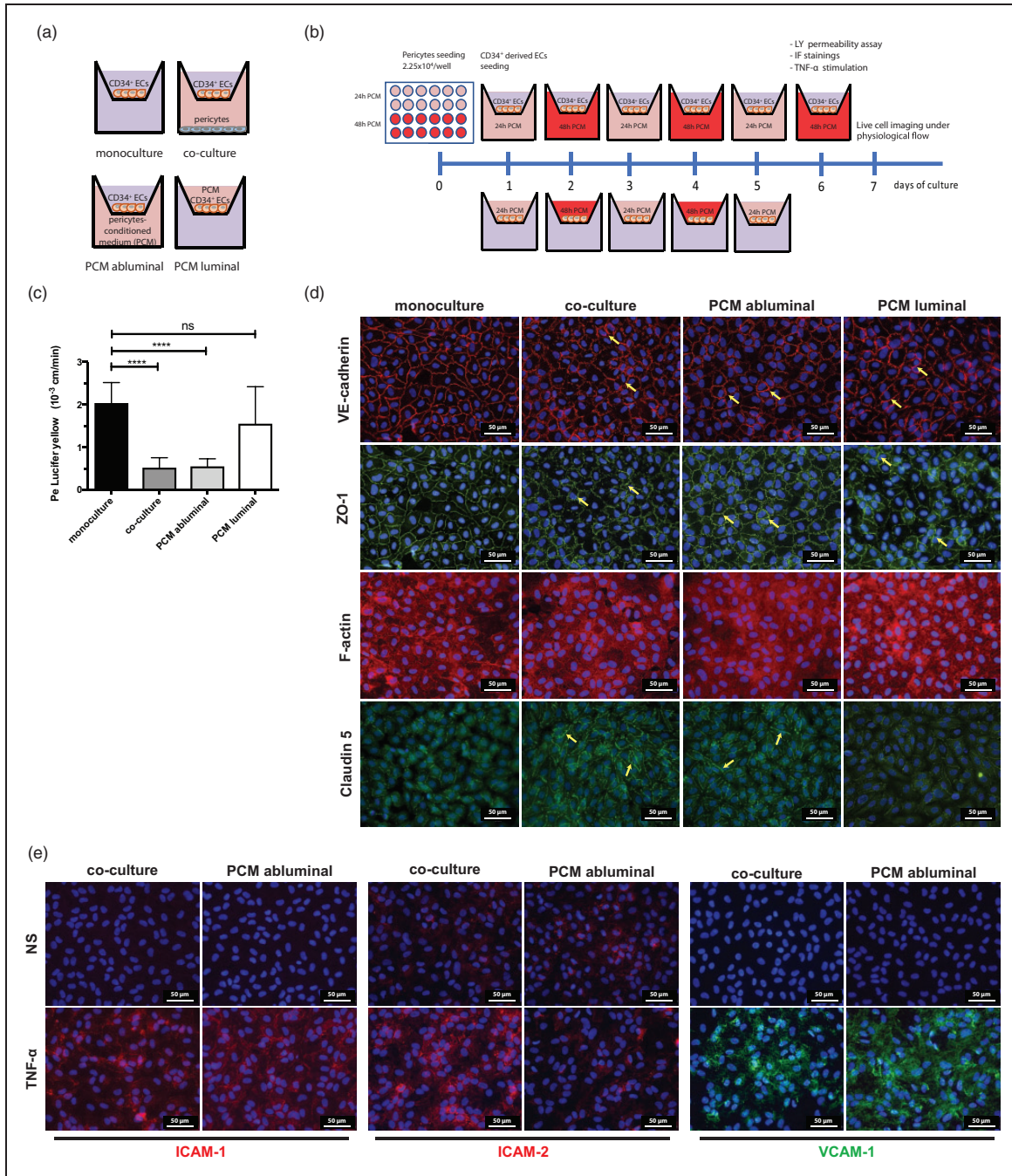


**Figure 2.** Induction of BBB characteristics in CD34<sup>+</sup> ECs by pericyte-conditioned medium. (a) Scheme of the different culture conditions used to test the BBB induction. (b) Timeline of experimental procedures: scheme of the PCM production and luminal or abluminal administration to the CD34<sup>+</sup>-derived ECs followed by Lucifer Yellow (LY) permeability assay, immunofluorescence stainings, and live cell imaging under physiological flow. (c) Lucifer Yellow (LY) permeability assay: the permeability was measured across monocultures of CD34<sup>+</sup>-derived ECs (monoculture), CD34<sup>+</sup>-derived ECs co-cultured with pericytes (co-culture), or pericyte-conditioned medium at the abluminal (PCM abluminal) or luminal (PCM luminal) side. Bars show means  $\pm$  SD of three independent experiments performed at least in duplicate for each condition. Statistical analysis: one-way ANOVA followed by Dunnett's multiple comparison test \*\*\*\* $p < 0.0001$ . (d) Immunofluorescence stainings for the junctional proteins VE-cadherin (red), ZO-1 (green), claudin-5 (green) and for F-actin (red) in CD34<sup>+</sup>-derived ECs grown in monoculture, in co-culture with pericytes or with PCM administered at the abluminal or luminal side are shown. The pictures show a more jagged VE-cadherin and ZO-1 fluorescent staining in the co-culture and PCM conditions (arrows). The claudin-5 staining is also more prominent and continuous in the co-culture and PCM abluminal conditions (arrows). Scale bar, 50  $\mu$ m. (e) Immunofluorescence staining for ICAM-1 and ICAM-2 (red), VCAM-1 (green), on CD34<sup>+</sup>-derived ECs grown in co-culture with pericytes or with PCM administered at the abluminal side, non-stimulated (NS) or stimulated with TNF- $\alpha$  for 16 h. Scale bar, 20  $\mu$ m.

side-by-side by testing the permeability of the EC monolayers for the small molecular weight tracer LY (Figure 2(c)). In accordance to our previous findings, the monoculture of CD34<sup>+</sup>-derived ECs did not establish a diffusion barrier for LY (Pe LY =  $2.04 \pm 0.48 \times 10^{-3}$  cm/min), while the co-culture with pericytes established BLECs with tight barrier characteristics as shown by the significantly reduced clearance of LY across the EC monolayer (Pe LY =  $0.52 \pm 0.23 \times 10^{-3}$  cm/min; Figure 2(c)). PCM applied from the abluminal side of the CD34<sup>+</sup>-derived EC monolayer-induced barrier characteristics comparable to those induced by the pericyte-co-culture (Pe LY =  $0.55 \pm 0.18 \times 10^{-3}$  cm/min; Figure 2(c)). Interestingly, applying PCM from the luminal side failed to induce comparable barrier characteristics underscoring that our in vitro model of the BBB appropriately mimics the in vivo situation with highly polarized ECs.

To confirm junctional integrity and maturation, EC monolayers were immunostained for the transmembrane adherens and tight junction proteins VE-cadherin and claudin-5, respectively, and the junctional scaffolding protein ZO-1. Abluminal application of PCM induced a junctional architecture in CD34<sup>+</sup>-derived ECs comparable to that induced by co-culture with bovine pericytes.<sup>15</sup> Specifically, the pericyte co-culture or the abluminally administered PCM induced a continuous and more jagged staining of the junctional and scaffolding proteins VE-cadherin and ZO-1 compared to the monoculture and PCM luminal conditions (Figure 2(d)). Moreover, junctional claudin-5 immunostaining was enhanced in BLECs under conditions of pericyte co-culture and in the abluminally administered PCM conditions (Figure 2(d)) when compared to controls. F-actin staining revealed the absence of stress fibers underscoring the quiescent nature of the ECs monolayers (Figure 2(d)). Also, BLECs in co-culture with pericytes or with abluminal PCM showed comparable upregulation of adhesion molecules such as ICAM-1 and VCAM-1 but not of ICAM-2 upon addition of a pro-inflammatory stimulus, e.g. by addition of TNF- $\alpha$  (Figure 2(e)). Taken together, these results show that differentiation of CD34<sup>+</sup>-derived ECs into BLECs can be achieved by applying PCM to the abluminal side.

**CD34<sup>+</sup>-derived ECs establish BBB characteristics when grown on NPN membranes.** In a next step, we asked if PCM-induced barrier characteristics in CD34<sup>+</sup>-derived ECs also occurred when the cells were grown on NPN membranes. The silicon chip platform of nanomembranes makes it easy to create customized, tightly bonded microfluidic devices using layer-by-layer assembly and ozone-based activation of silicone/PDMS layers.<sup>46,47</sup> Thus, for these purposes, we fabricated a “Transwell®

mimetic”, in which an NPN membrane divides an upper and lower compartment in static culture (Figure 3(a)). The membrane compartment of this device is open for media and reagent application from the top and promotes easy gas exchange for maintaining physiological pH within the media. The basal compartment can be accessed from fluid ports on the top of the device and is separated from the membrane compartment by the NPN membrane providing the sole area for exchange of factors between compartments. The entire device can be autoclaved and the volume requirements in the upper and lower compartments are only 50  $\mu$ L and 20  $\mu$ L, respectively.

In order to induce barrier characteristics in CD34<sup>+</sup>-derived ECs, we followed the same culture procedure as depicted in Figure 2(b). CD34<sup>+</sup>-derived ECs ( $1 \times 10^5$  cells/mL) were seeded on the Matrigel-coated NPN membrane and grown in the absence or presence of PCM applied in the basal compartment (Figure 3(b)). CD34<sup>+</sup>-derived ECs were cultured for five days replacing the PCM in the basal compartment every 24 h while alternating the 24 h and 48 h PCM. Barrier characteristics were tested after five days of culture by performing an LY permeability assay (Figure 3(b)). The paracellular permeability of EC monolayers was evaluated as described in Supplementary Methods, and the PSe was divided by a cell growing area (0.014 cm<sup>2</sup>), in order to generate the endothelial Pe in cm/min. While CD34<sup>+</sup>-derived ECs grown on NPN membranes in monocultures did not establish a tight barrier (Pe LY =  $1.82 \pm 0.60 \times 10^{-3}$  cm/min), in the presence of abluminal PCM, CD34<sup>+</sup>-derived ECs grown on NPN membranes established BLEC characteristics (Pe LY =  $0.39 \pm 0.24 \times 10^{-3}$  cm/min; Figure 3(b)), comparable to BLECs grown on Transwell® filter inserts (Figure 2(a)). Induction of BLEC properties grown on NPN membranes by abluminal PCM was further confirmed by the junctional localization of VE-cadherin, claudin-5, and ZO-1 (Figure 3(c)). Thus, NPN membranes are suitable for the induction of BBB properties by PCM in CD34<sup>+</sup>-derived ECs.

Next, we investigated cell surface expression of adhesion molecules known to mediate T-cell interaction with the BBB on BLECs grown on the NPN membranes. We found constitutive cell surface expression of the adhesion molecule ICAM-2, constitutively expressed in human ECs<sup>48</sup> and to a lesser degree for ICAM-1 but not of VCAM-1 on BLECs (Figure 3(d)). To mimic an inflammatory environment, BLECs were stimulated with tumor necrosis factor alpha (TNF- $\alpha$ ) (10 ng/mL) for 16 h which resulted in up-regulation of ICAM-1 and VCAM-1, as demonstrated in our previous work.<sup>17</sup> Moreover, TNF- $\alpha$  stimulation induced the formation of F-actin stress



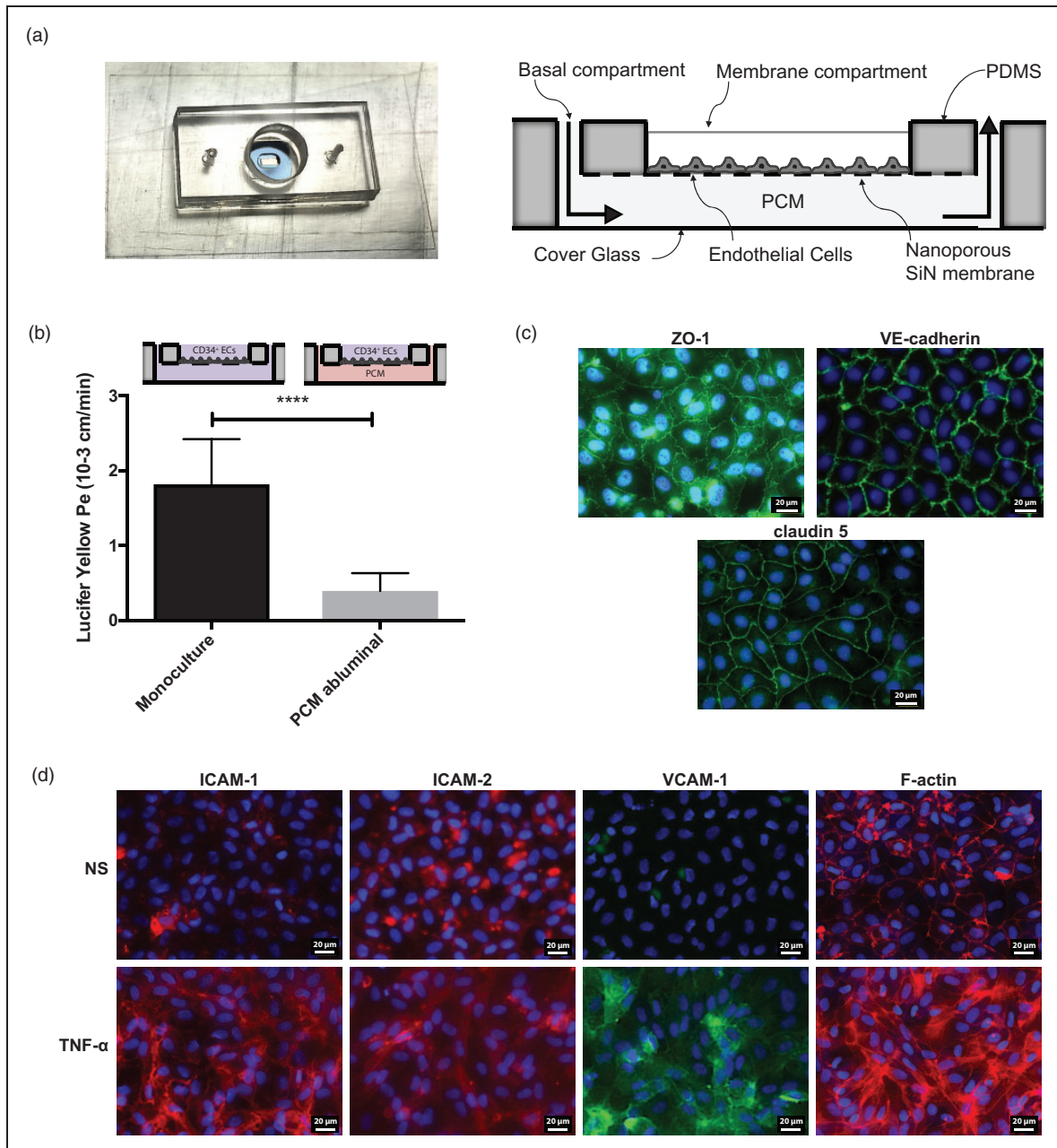


**Figure 3.** CD34<sup>+</sup>-derived ECs grown on nanoporous silicon nitride membranes establish BLECs characteristics. (a) Design of a “Transwell mimetic” device developed to culture CD34<sup>+</sup>-derived ECs in the membrane compartment of the NPN membrane, in close proximity to the pericyte-conditioned medium (PCM) in the basal compartment. The device is constructed from poly dimethyl siloxane (PDMS) and silicone gaskets sandwiched together using UV-ozone bonding. Note the transparent nature of the whole device in general, and specifically of the silicon membrane used to support cell growth. The schematic is shown on the right (drawn not to scale). Molecular tracers can be added to the membrane compartment and collected from the basal compartment for fluorometric analysis. (b) The permeability Lucifer Yellow (PeLY) was measured across monolayers of CD34<sup>+</sup>-derived ECs grown alone (monoculture) and CD34<sup>+</sup>-derived ECs cultured in the presence of PCM in the abluminal compartment. The values show mean  $\pm$  SD of 11 customized devices for the CD34<sup>+</sup>-derived ECs mono-cultures and 12 devices for the CD34<sup>+</sup> ECs cultured in the presence of abluminal PCM. Statistical analysis: Student’s t-test \*\*\*\* $p < 0.0001$ . (c) Immunofluorescence staining on BLECs induced by PCM in the basal compartment, for the junctional markers ZO-1 (green), VE-cadherin (green) and claudin-5 (green). Each staining is representative of two independent experiments performed on two distinct devices, Scale bar, 20  $\mu$ m. (d) Immunofluorescence staining for ICAM-1 and ICAM-2 (red), VCAM-1 (green), and F-actin (red) on BLECs unstimulated (NS) or stimulated with TNF- $\alpha$  for 16 h. Each staining is representative of two independent experiments performed on two distinct devices. Scale bar, 20  $\mu$ m.

fibers as revealed by the immunofluorescence staining (Figure 3(d)). Taken together, these results show that our human *in vitro* BBB model is functionally reproduced on NPN and suitable to investigate the role of the signature molecules involved in T-cell trafficking.

**Establishment of a small-scale human *in vitro* BBB model under flow: Introduction of the  $\mu$ SiM-CVB flow system.** Using the same layer-by-layer fabrication used for open “Transwell<sup>®</sup> mimetics,” we constructed a closed, two-chamber flow device, which we refer to as “ $\mu$ SiM-CVB flow system” (Figure 4(a)). This new device is composed of several 300  $\mu$ m thick silicone layers that create the compartments necessary for the apical growth of the CD34<sup>+</sup>-derived ECs and the abluminal application of PCM. The CD34<sup>+</sup>-derived ECs are seeded on the silicon nanomembrane via the top channel that also serves as the flow channel. In addition, reservoirs have been added to the top PDMS block of the device at both ends of each channel. This allows the addition of excess culture medium (200  $\mu$ L per channel) to prevent evaporation during prolonged cell culture (Figure 4(b)). In order to grow the BLECs monolayer, CD34<sup>+</sup>-derived ECs are seeded in the top channel on the silicon nanomembrane (1.4 mm<sup>2</sup>) at a concentration of  $1 \times 10^6$  cells/mL. Induction of BLECs is achieved by the daily and alternating administration of 24 h and 48 h PCM for six days under static conditions, as established in the “Transwell<sup>®</sup> mimetic” system. The differentiation of CD34<sup>+</sup> EC to BLECs in the  $\mu$ SiM-CVB flow system by application of PCM into the lower chamber could be confirmed by the induction of permeability values to LY (Pe LY =  $0.72 \pm 0.13 \times 10^{-3}$  cm/min) comparable to Pe LY values for BLECs induced with abluminal PCM in the standard Transwell<sup>®</sup> inserts and Transwell<sup>®</sup> mimetics (Supplemental Figure S2). Furthermore, the junctional localization of VE-cadherin, claudin-5, and ZO-1 confirmed the BLECs junctional maturation by abluminal application of PCM in the  $\mu$ SiM-CVB flow system (Figure 4(c)).

To apply flow on the BLEC monolayer, both ends of the top channels are connected to transparent PVC tubing with the help of 18-gauge straight needles with the tap open to avoid any increased pressure in the chamber. The inlet tubing is then connected to a three-way tap linked to two reservoirs, respectively, containing the Th1 cell suspension and migration assay medium, and the outlet tubing was connected to a programmable pump.

With this device and scheme, it was possible to superfuse the Th1 cells over the BLEC monolayer and directly image the T cells in phase contrast with a transmitted light-inverted microscope equipped with a temperature-controlled chamber (37°C), and to observe the multi-step

T-cell migration across the BBB under physiological flow *in vitro* (scheme in Figure 4(d)). To perform the flow experiment, first, the Th1 cells were infused in the top channel for 4 min at a low flow rate of 0.1 dyne/cm<sup>2</sup> to allow a first contact with the BLECs (accumulation phase). Then, the migration assay medium only was infused, and the flow rate was increased to 1.5 dyne/cm<sup>2</sup> to reach a physiological shear for 30 min (shear phase) allowing the study of post-arrest T-cell behavior on the BLECs monolayer. In order to see if we could image the BLECs at high resolution and keep the focus on the cells for the duration of the flow experiment, a temporal snapshot of the BLECs taken from a video recorded with a 10 $\times$  magnification was made, showing the first and last frame of a flow movie (Figure 4(e)). In order to mimic conditions of the BBB under inflammatory or non-inflammatory conditions, BLECs were pre-treated or not with TNF- $\alpha$  after five days of culture with the PCM, when the BBB characteristics (low permeability, mature tight junctions) were established (Figure 3(b) and (c)), 16 h before starting the flow experiment. First, we found that the resolution was sufficient to perfectly distinguish each EC in phase contrast images. We observed that treatment of BLECs with TNF- $\alpha$  induced a more elongated shape of the BLECs before flow application (Figure 4(e)), which is in accordance with the induction of F-actin stress fibers as observed with the immunofluorescence staining (Figure 3(d)). When starting to apply flow (0 min), the NPN membrane’s stiffness kept it perfectly in focus (34 min 55 s) and allowed us to continuously image the BLEC monolayer under physiological flow in the same focal plane. In addition, we ensured that the monolayer stayed perfectly intact and in focus under physiological flow for a time period of at least 30 min, which is a prerequisite for following the T cell-BLECs interactions over time.

**Live cell imaging of the interaction of human T cells with BLECs under physiological flow.** In a final step, we employed the  $\mu$ SiM-CVB to study the interaction of human T cells with the human BBB under physiological flow following the same procedure described above. In order to illustrate how we could observe various types of T cell/BLEC interactions with high resolution, we generated temporal snapshots from a video recorded with a 20 $\times$  magnification where BLECs were stimulated with TNF- $\alpha$  (Figure 5(a)). In addition, we also recorded videos with a 10 $\times$  magnification of T cell-BLEC interactions where BLECs were stimulated (video 2, see <http://journals.sagepub.com/home/jcb>) or not (video 1, see <http://journals.sagepub.com/home/jcb>) with TNF- $\alpha$ . These videos allowed us to have a statistical comparison of the T-cell behavior on the BLEC monolayers in unstimulated and TNF- $\alpha$ -stimulated conditions (Figure 5(b)), since a higher number of T

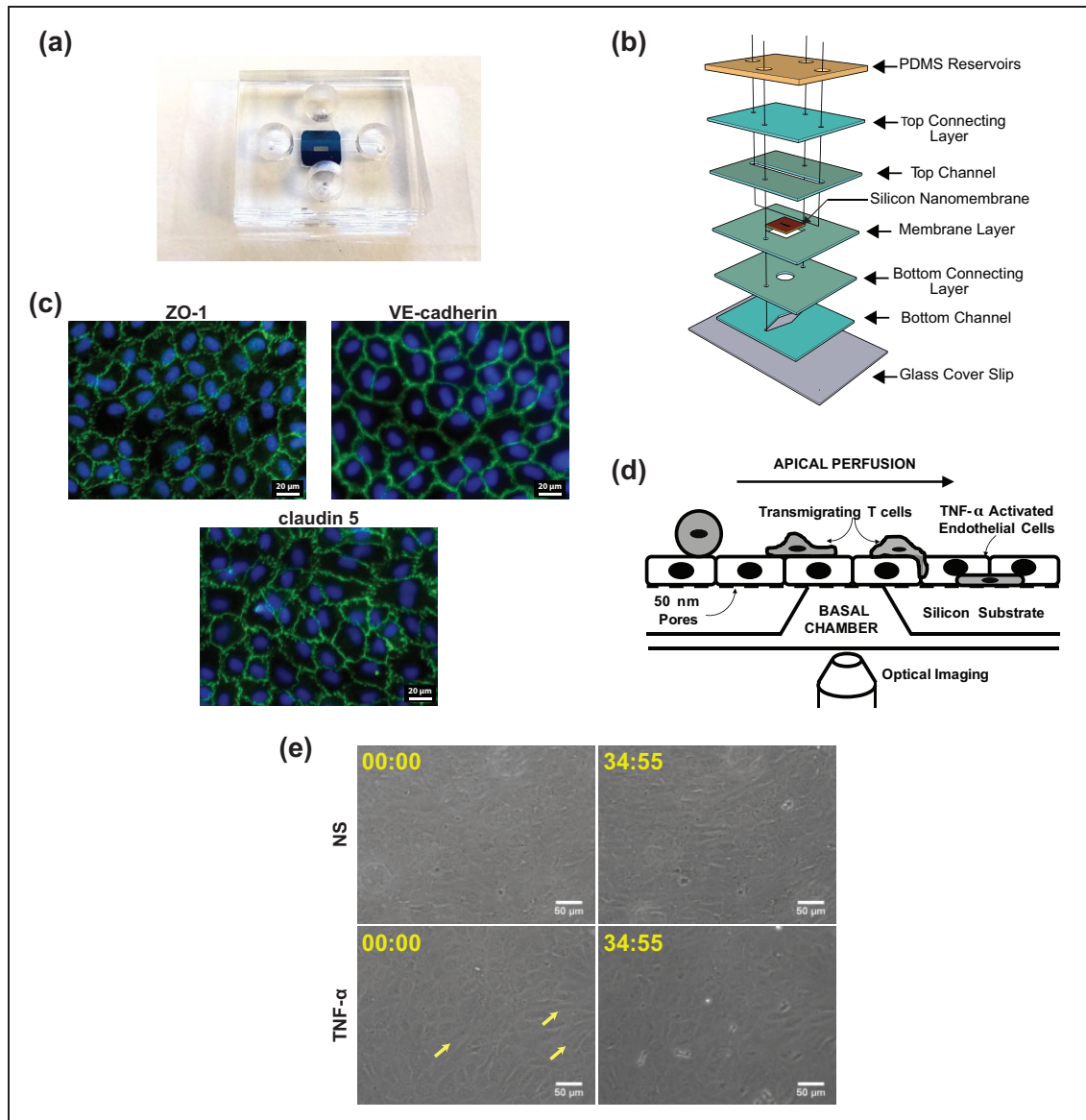


**Figure 4.** Assembly of the  $\mu$ SiM-CVB flow system. (a) Photograph and (b) exploded view of the assembled  $\mu$ SiM-CVB flow system. Note the optical transparency of the assembled device components. The supporting layer of the device is a thin #1.5 glass cover slip. All the silicone layers (blue/green/teal) are 300  $\mu$ m thick. “Top” and “Bottom” channels perfuse media, while the “Top Connecting Layer” and “Bottom Connecting Layer” demarcate the top and bottom compartments, respectively. The “Membrane Layer” provides a supporting framework for the membrane. The topmost PDMS reservoirs store the excess media and are exposed to the outside-incubator environment for gas exchange. Similarly, all the other device components are all gas-permeable and are sterilized by autoclaving. During flow set-up, the 18 gauge needles fitted with silicone tubings are inserted in the four holes in the Top Connecting Layer. (c) Immunofluorescence staining on BLECs grown in the  $\mu$ SiM-CVB flow system, induced by PCM in the basal compartment, for the junctional markers ZO-1 (green), VE-cadherin (green) and claudin-5 (green). Each staining is representative of two independent experiments performed on two distinct devices, Scale bar, 20  $\mu$ m. (d) Schematic of the settings for live cell imaging of the T cell/BLEC interactions under flow. T cells are perfused on the apical (top) side of the device and migrate in a multi-step process across the BLEC monolayer. T cells can also crawl in the subendothelial layer above the membrane. The 50-nm pores in the silicon membrane prevent their passage into the basal (bottom) compartment of the device. The working distance of the device (distance between microscope objective and T cells) is 1.180 mm. (e) A temporal snapshot to illustrate the resolution and focusing-stability under flow from two videos recorded at 10 $\times$  magnification (EC Plan-Neofluar 10 $\times$ /0.30 Ph1). BLECs were cultured and TNF-activated as described in the main text. The pictures show the BLECs to illustrate image clarity and the stability of focus from the start (00 min) to the end (34 min 55 s) of the recording session under flow. The arrows show area where the BLECs are elongated after stimulation with TNF- $\alpha$ . The time is displayed on the top left of the video (min:s format). Scale = 50  $\mu$ m.



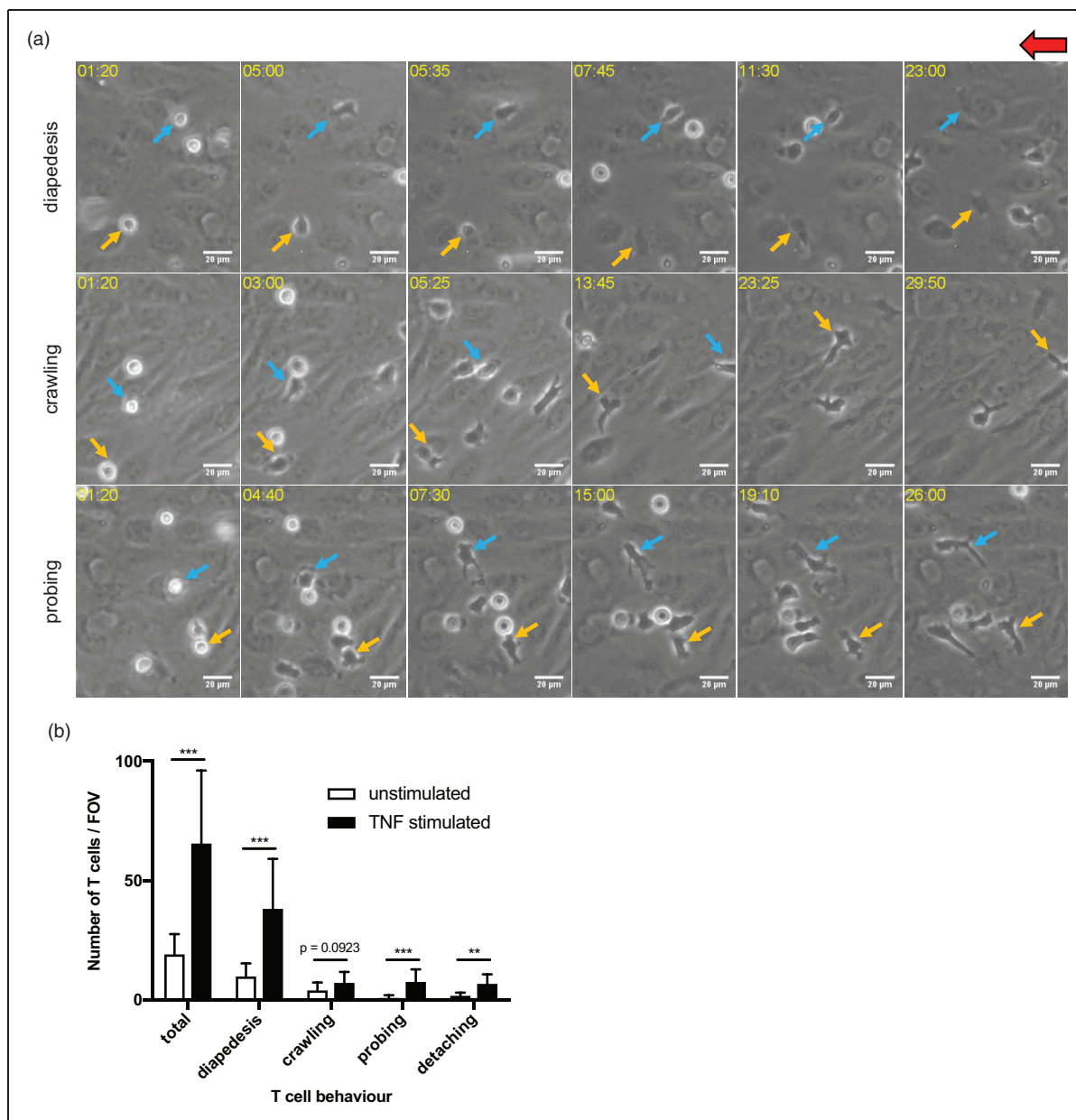


**Figure 5.** In vitro live cell imaging of the T cell-BBB interactions under flow. (a) A temporal snapshot illustrating that the different T cell-BLECs interactions have been made with several frames taken from a video recorded with a 20× magnification (LD Plan-Neofluar 20×/0.4 Korr Ph2). The CD34<sup>+</sup> ECs were cultured in the top channel of the flow chamber with the PCM in the bottom channel for six days, and the CD34<sup>+</sup> ECs were stimulated with TNF (10 ng/mL) 16 h before starting to record the video. Th1 cells are allowed to accumulate on the BLECs monolayer at a low flow rate of 0.1 dyne/cm<sup>2</sup> for 4 min from the first frame after the first Th1 cells appear in the field of view, then the flow rate was set to 1.5 dyne/cm<sup>2</sup> for 30 min (shear phase). Each row is showing a specific behavior of the Th1 cells with the BLECs with the example of two different cells one highlighted with a blue arrow and the other one with a yellow arrow. The first row illustrates the diapedesis event where T cells start to arrest (1 min 20 s) and then polarize and firmly adhere (5 min) to the BLECs. Then, the T cells start to transmigrate through the BLECs monolayer (5 min 35 s) and take more (23 min, blue arrow) or less (7 min 45 s, yellow arrow) time to complete diapedesis. The pore size of 50 nm prevents the leukocytes from crossing the silicon membrane; cells are trapped in the subendothelial spaces and can still be followed and identified by their darker gray shape in comparison of the BLECs monolayer (23 min). The second row illustrates the crawling event where T cells first arrest (1 min 20 s) and then polarize and firmly adhere (3 min) to the BLECs. Then, the T cells start to form a leading edge with a lot of small protrusions (5 min 25 s, blue arrow and 13 min 45 s, yellow arrow) and actively move on the BLECs against the direction of the flow until they even disappear from the field of view (13 min 45 s, blue arrow and 29 min 50 s, yellow arrow). The third row illustrates the probing event where T cells first arrest (1 min 20 s) and then polarizes and firmly adheres (4 min 40 s) to the BLECs. Then, the T cells remained

(continued)



cells could be tracked compared to higher magnification videos, at the cost of a lower resolution. To analyze the respective T-cell behavior on the BLECs monolayers in a quantitative manner, we performed a visual frame-by-frame offline analysis of the time-lapse videos. To this end, each T cell was categorized into a specific behavioral group. Under both, unstimulated and TNF- $\alpha$ -stimulated conditions, the majority of T cells were found to polarize upon arrest (videos 1 and 2) and to migrate across the BLEC monolayer with or without prior crawling on the BLECs. These were categorized under “diapedesis” (Figure 5(a)). T cells that crawled on the surface of the BLECs for the entire observation time were categorized as “crawling” (videos 1 and 2, Figure 5(a)). One additional behavior observed was T cells that remained stationary without displacing beyond a distance exceeding their own diameter and presenting dynamic cellular protrusions and thus “probing” the BLEC monolayer (videos 1 and 2, Figure 5(a)). Also, some T cells were found to quickly “detach” from the BLECs monolayer when the flow rate increased at the beginning of the shear phase (video 2). In general, we observed a higher number of T cells arresting on the TNF- $\alpha$ -stimulated BLECs versus the non-stimulated BLECs monolayers, resulting in an increased number of T cells interacting with the TNF- $\alpha$  stimulated BLECs in each T-cell behavioral category (Figure 5(b)). Overall, the TNF- $\alpha$  stimulation favored T cell-BLECs interactions without modulating their behavior among categories. This observation is in accordance with the upregulated cell surface expression of ICAM-1 and VCAM-1 previously shown (Figure 3(d)), suggesting that upon TNF- $\alpha$  stimulation, the upregulation of adhesion molecules could explain the significantly higher number of Th1 cells found to arrest on BLECs under physiological flow,  $\sim 4$  min after starting to infuse T cells and just after the accumulation phase (Figure 5(b)). Taken together, our novel  $\mu$ SiM-CVB flow system allows for detailed observation of the multi-step T-cell extravasation across a human model of the BBB at a very small scale suitable for employing rare patient-derived immune cells.

## Discussion

The development of an in vitro platform to study the migration of immune cells across the BBB in the context of human CNS disorders has provided many challenges. We began addressing these challenges by first establishing a novel human in vitro model of the BBB from human ECs derived from cord blood CD34<sup>+</sup> hematopoietic stem cells.<sup>15</sup> We demonstrated that when cocultured with pericytes, CD34<sup>+</sup> EC differentiate into BLECs establishing low permeability barriers and mature tight junctions. Due to the general availability of cord blood stem cells, BLECs can be widely adopted to study molecular mechanisms in pathologies, implicating the BBB such as neurodegenerative or neuroinflammatory disorders (e.g. Alzheimer’s disease, multiple sclerosis), stroke and traumatic brain injury, infectious processes, and inflammatory pain.

While we have previously used BLECs to study immune cell extravasation and cancer metastatic cells across the BBB in static culture conditions,<sup>16,17,49</sup> the application of flow is needed for more physiological observations.<sup>8,25</sup> The visualization of the multi-step immune cell extravasation across the vascular wall requires a testing platform compatible with transmitted light microscopy, preferably phase contrast. The desire for flow and live cell imaging has compelled us and others to use flow chambers with ECs cultured on glass coverslips, as the track-etched membranes used in traditional two-chamber filter devices are notoriously bad for imaging under transmitted light.<sup>44</sup> This choice, however, introduces new complications as non-permeable substrates are thought to compromise the polarization of barrier cells due to the lack of basal transport.<sup>50</sup> In addition, these flow chambers are not suitable for in vitro BBB models that rely on the continuous and polarized cross-talk of the brain ECs with cellular or acellular elements of the neurovascular unit, such as pericytes or astrocytes and CNS-derived factors, respectively.<sup>51,52</sup>

The previous decade has witnessed the emergence of customized microsystems for “organ-on-chip” models or “microphysiological systems”.<sup>53</sup> While a number of these efforts have focused on BBB,<sup>36–39,41</sup> only Walter et al.<sup>54</sup> addressed the need for membrane transparency.

### Figure 5. Continued

stationary without displacing beyond a distance exceeding their own diameter and presenting the ability to greatly modulate their shape, sending a lot of dynamic cellular protrusions around them (from 7 min 30 s to 26 min). The red arrow shows the direction of flow and the time is displayed on the top left of the video (min:s format). Scale = 20  $\mu$ m. (b) Analysis of the arrest and post-arrest T-cell interactions with NS and TNF- $\alpha$  stimulated BLECs in the field of view of the videos recorded with a 10 $\times$  magnification (example in videos 1 and 2) under physiological flow (1.5 dyne/cm<sup>2</sup>) for 30 min. T cells remaining arrested to the BLECs monolayer were quantified (total) at the end of the accumulation phase (0.1 dyne/cm<sup>2</sup> for 4 min from the time the first T cells appear in the field of view). Then post-arrest T cell behavior on the BLECs monolayer under flow was analyzed, such as each T cell was assigned to one of four categories as follows: diapedesis, crawling, probing, and detaching. Values are means  $\pm$  SD for 10 assays for each condition. Statistical analysis: t-test \* $p$  < 0.05, \*\* $p$  < 0.01,  $p$  < 0.001, \*\*\* $p$  < 0.0001.

Their solution was to employ “transparent” track etched membranes that have 100 fold fewer pores than conventional materials ( $10^6$  pores/cm<sup>2</sup> vs.  $10^8$  pores/cm<sup>2</sup>) and are more than twice as thick (23  $\mu$ m vs. 6–10  $\mu$ m). While these membrane modifications diminish the confounding influence of pores on light transmission and enabled clear phase images of monolayers, they also dramatically reduce the diffusive permeability of the membranes by more than two orders of magnitude. Indeed, we calculated the small molecule permeability of the low porosity TE membranes used by Walter et al. to be  $10^{-5}$  cm/s, a value lower than some of the permeabilities we report here for LY transport across BLEC monolayers. Thus, these low porosity TE membranes improve imaging, but can be rate limiting for small molecule transport between chambers.

We addressed the need for optical transparency by building the first in vitro barrier models featuring NPN.<sup>26</sup> NPN is a durable and highly manufacturable “silicon nanomembrane,” a family of ultrathin free-standing porous membranes produced by silicon micro-fabrication methods.<sup>28,43,55</sup> NPN membranes are 50 nm thick with  $\sim$ 40 nm pores and a density of  $10^{10}$  pores/cm<sup>2</sup>.<sup>26</sup> The small molecule diffusive permeability of these membranes is a remarkable  $\sim$ 0.1 cm/s,<sup>56</sup> a value so high that is indistinguishable from free diffusion through water in practical assays.<sup>27</sup> For our purposes, NPN is also superior to the microporous SiO<sub>2</sub> nanomembranes previously used to visualize direct HUVEC/ADSC co-cultures<sup>43</sup> because: (1) The sub-optical pore sizes of NPN give a feature-free background for high-quality visualizing immune cell/endothelial interactions; (2) EC adhesion to NPN is excellent even under high levels of shear stress that readily strips ECs from microporous SiO<sub>2</sub> (Figure S1).

In addition to their extraordinary permeability, NPN membranes were superior to any commercially available membrane we tested with respect to their optical characteristics and adhesive properties. Indeed, the CD34<sup>+</sup> ECs grew perfectly on the NPN membrane reaching confluency 24 h after seeding and building a dense monolayer after six days of culture that allowed maintenance of a BLEC monolayer under physiological flow. Because the silicon platform enables the facile construction of dual compartment culture devices, we readily adapted the co-culture-based human in vitro BBB model requiring co-culture of CD34<sup>+</sup> ECs with pericytes.<sup>15</sup> Successful replacement of the pericyte co-culture with PCM in the basal compartment further advanced the in vitro BBB model by eliminating contributions from out-of-focus cells when imaging the endothelial layer. Using PCM instead of the standard co-culture with pericytes revealed only one minor difference with respect to a lack of up-regulated expression of ICAM-2 upon stimulation of BLECs with TNF- $\alpha$ . However, since ICAM-1 is the

major and high-affinity ligand for LFA-1 on T cells, this result does not invalidate our model to study immune cell trafficking. Moreover, regarding the difference in the model’s characteristics, we noticed that after the transfer of the BLECs from the “Transwell® mimetic” to the  $\mu$ SiM-CVB flow system, the claudin-5 staining appeared more jagged, which could be a sign of a different junctional maturation. Since we measured comparable permeability values of the BLEC monolayer in the two devices, it seems that this does not have a significant impact on the paracellular tightness that could modify immune cell interactions with the BLECs. However, this observation may become important when adapting this in vitro BBB model for small molecule permeability screenings.

The next step, which was to apply flow in our  $\mu$ SiM-CVB flow system, took full advantage of the properties of the NPN material that help distinguish it from all commercial membrane materials. While its nanoscale thinness gives NPN high permeability and makes it excellent for live cell imaging, we also found that the ceramic-like membrane is still sufficiently stiff that it remains in focus with the onset of flow and throughout more than 30 min of continuous recording. The optical imaging quality of T-cell interactions observed on the BLECs monolayer using the novel  $\mu$ SiM-CVB flow system were indistinguishable from those on glass.<sup>32,57,58</sup> The  $\mu$ SiM-CVB flow system traps T cells below the BLEC monolayer, which does not allow for easy T-cell collection and may have consequences for the experimental outcomes. Artificial T cell accumulation, e.g. when investigating chemokine gradients can be avoided by modifying the T-cell numbers superfused over the BLEC monolayer and the time of recording.

Despite current trends toward increasing complexity in the development of microphysiological systems, it was not our goal to achieve an anatomical mimetic of the human BBB by including all the cellular and acellular elements of the neurovascular unit. Instead, we focused on addressing a specific unmet need in the CVB research community: an in vitro platform that enables the observation of live human immune cells interacting with a well-characterized human BBB model under flow. The observations of T-cell arrest, crawling on, and diapedesis across the BLECs monolayer under physiological flow as well as the observed influence of the inflammatory status of BLECs on these interactions, validates the  $\mu$ SiM-CVB for these purposes. Simplicity, such as the elimination of the need for co-culture, is one benefit of our platform. Moreover, the volumes of the apical channels of both the “Transwell® mimetic” and the  $\mu$ SiM-CVB flow system are less than 20  $\mu$ L, a feature that will eventually allow the use of small samples of body fluids or cells obtained from patients for personalized medicine. Overall, we expect the  $\mu$ SiM-CVB platform to

open new opportunities to define novel therapeutic targets for neurological disorders ranging from neuroinflammation and neurodegeneration to tumor metastasis and for adaptation to investigate other cellular barriers.

### Acknowledgements

We gratefully acknowledge Thomas Andolsek for the initial phase of device manufacturing and the support of the Microscopy Imaging Center of the University of Bern. We further acknowledge Daniela Latorre and David Jarrossay for their valuable help in purifying the T cells.

### Author's contributions

Britta Engelhardt: conceptualization; resources; supervision; funding acquisition; project administration; writing—review and editing. Adrien Mossu: data curation; formal analysis; investigation; methodology; writing—original draft. Maria Rosito: data curation; formal analysis; investigation; methodology; writing—original draft. Tejas Khire: data curation; formal analysis; investigation; methodology; writing—original draft. Hung Chung: data curation; methodology. Hideaki Nishihara: data curation; formal analysis; investigation; methodology. Isabelle Gruber: Data curation; formal analysis; investigation; methodology. Emma Luke: methodology. Lucie Dehouck: resources; methodology. Federica Sallusto: resources; methodology. Fabien Gosselet: resources; methodology; writing—review and editing. James McGrath: conceptualization; supervision; funding acquisition; project administration; writing—review and editing.

### Declaration of conflicting interests

The author(s) declared the following potential conflicts of interest with respect to the research, authorship, and/or publication of this article: J.L.M. declares a competing financial interest as a co-founder and equity holder of SiMPore Inc., a commercial manufacturer of NPN and other silicon-based membrane materials.

### Funding

The author(s) disclosed receipt of the following financial support for the research, authorship, and/or publication of this article: This study was funded by the Swiss National Science Foundation (CRSII3\_154483, Sinergia UnmetMS) to BE and FS, the Swiss Multiple Sclerosis Society to AM and the Germaine de Stael PHC program to FG and BE. JLM and TK were supported by NIH R01 HL125265.

### ORCID iD

Adrien Mossu  <http://orcid.org/0000-0001-5986-2762>

### Supplementary material

Supplementary material for this paper can be found at the journal website: <http://journals.sagepub.com/home/jcb>

### References

- Engelhardt B and Sorokin L. The blood-brain and the blood-cerebrospinal fluid barriers: function and dysfunction. *Semin Immunopathol* 2009; 31: 497–511.
- Engelhardt B and Ransohoff RM. Capture, crawl, cross: the T cell code to breach the blood-brain barriers. *Trends Immunol* 2012; 33: 579–589.
- Sospedra M and Martin R. Immunology of multiple sclerosis. *Semin Neurol* 2016; 36: 115–127.
- Diebold M and Derfuss T. Immunological treatment of multiple sclerosis. *Semin Hematol* 2016; 53(Suppl 1): S54–S57.
- Martin R, Sospedra M, Rosito M, et al. Current multiple sclerosis treatments have improved our understanding of MS autoimmune pathogenesis. *Eur J Immunol* 2016; 46: 2078–2090.
- Helms HC, Abbott NJ, Burek M, et al. In vitro models of the blood-brain barrier: an overview of commonly used brain endothelial cell culture models and guidelines for their use. *J Cereb Blood Flow Metab* 2016; 36: 862–890.
- Grant GA, Abbott NJ and Janigro D. Understanding the physiology of the blood-brain barrier: in vitro models. *News Physiol Sci* 1998; 13: 287–293.
- Steiner O, Coisne C, Engelhardt B, et al. Comparison of immortalized bEnd5 and primary mouse brain microvascular endothelial cells as in vitro blood-brain barrier models for the study of T cell extravasation. *J Cereb Blood Flow Metab* 2011; 31: 315–327.
- Cayrol R, Haqqani AS, Ifergan I, et al. Isolation of human brain endothelial cells and characterization of lipid raft-associated proteins by mass spectroscopy. *Methods Mol Biol* 2011; 686: 275–295.
- Weksler BB, Subileau EA, Perriere N, et al. Blood-brain barrier-specific properties of a human adult brain endothelial cell line. *FASEB J* 2005; 19: 1872–1874.
- Eigenmann DE, Xue G, Kim KS, et al. Comparative study of four immortalized human brain capillary endothelial cell lines, hCMEC/D3, hBMEC, TY10, and BB19, and optimization of culture conditions, for an in vitro blood-brain barrier model for drug permeability studies. *Fluids Barriers CNS* 2013; 10: 33.
- Deli MA, Abraham CS, Kataoka Y, et al. Permeability studies on in vitro blood-brain barrier models: physiology, pathology, and pharmacology. *Cell Mol Neurobiol* 2005; 25: 59–127.
- Canfield SG, Stebbins MJ, Morales BS, et al. An isogenic blood-brain barrier model comprising brain endothelial cells, astrocytes, and neurons derived from human induced pluripotent stem cells. *J Neurochem* 2017; 140: 874–888.
- Lippmann ES, Al-Ahmad A, Palecek SP, et al. Modeling the blood-brain barrier using stem cell sources. *Fluids Barriers CNS* 2013; 10: 2.
- Cecchelli R, Aday S, Sevin E, et al. A stable and reproducible human blood-brain barrier model derived from hematopoietic stem cells. *PLoS One* 2014; 9: e99733.
- Vandenhoute E, Drolez A, Sevin E, et al. Adapting coculture in vitro models of the blood-brain barrier for use in cancer research: maintaining an appropriate endothelial



- monolayer for the assessment of transendothelial migration. *Lab Invest* 2016; 96: 588–598.
17. Lyck R, Lecuyer MA, Abadier M, et al. ALCAM (CD166) is involved in extravasation of monocytes rather than T cells across the blood-brain barrier. *J Cereb Blood Flow Metab* 2017; 37: 2894–2909.
  18. Coisne C, Lyck R and Engelhardt B. Live cell imaging techniques to study T cell trafficking across the blood-brain barrier in vitro and in vivo. *Fluids Barriers CNS* 2013; 10: 7.
  19. Martinelli R, Zeiger AS, Whitfield M, et al. Probing the biomechanical contribution of the endothelium to lymphocyte migration: diapedesis by the path of least resistance. *J Cell Sci* 2014; 127: 3720–3734.
  20. Shulman Z and Alon R. Real-time analysis of integrin-dependent transendothelial migration and integrin-independent interstitial motility of leukocytes. *Methods Mol Biol* 2012; 757: 31–45.
  21. Munir H, Rainger GE, Nash GB, et al. Analyzing the effects of stromal cells on the recruitment of leukocytes from flow. *J Vis Exp* 2015; 95: e52480.
  22. Garberg P, Ball M, Borg N, et al. In vitro models for the blood-brain barrier. *Toxicol In Vitro* 2005; 19: 299–334.
  23. Abbott NJ, Patabendige AA, Dolman DE, et al. Structure and function of the blood-brain barrier. *Neurobiol Dis* 2010; 37: 13–25.
  24. Cinamon G, Shinder V and Alon R. Shear forces promote lymphocyte migration across vascular endothelium bearing apical chemokines. *Nat Immunol* 2001; 2: 515–522.
  25. Schreiber TH, Shinder V, Cain DW, et al. Shear flow-dependent integration of apical and subendothelial chemokines in T-cell transmigration: implications for locomotion and the multistep paradigm. *Blood* 2007; 109: 1381–1386.
  26. DesOrmeaux JP, Winans JD, Wayson SE, et al. Nanoporous silicon nitride membranes fabricated from porous nanocrystalline silicon templates. *Nanoscale* 2014; 6: 10798–10805.
  27. Snyder JL, Clark A Jr, Fang DZ, et al. An experimental and theoretical analysis of molecular separations by diffusion through ultrathin nanoporous membranes. *J Memb Sci* 2011; 369: 119–129.
  28. Striemer CC, Gaborski TR, McGrath JL, et al. Charge- and size-based separation of macromolecules using ultrathin silicon membranes. *Nature* 2007; 445: 749–753.
  29. Pedroso DC, Tellechea A, Moura L, et al. Improved survival, vascular differentiation and wound healing potential of stem cells co-cultured with endothelial cells. *PLoS One* 2011; 6: e16114.
  30. Cecchelli R, Dehouck B, Descamps L, et al. In vitro model for evaluating drug transport across the blood-brain barrier. *Adv Drug Deliv Rev* 1999; 36: 165–178.
  31. Coisne C, Dehouck L, Faveeuw C, et al. Mouse syngenic in vitro blood-brain barrier model: a new tool to examine inflammatory events in cerebral endothelium. *Lab Invest* 2005; 85: 734–746.
  32. Steiner O, Coisne C, Cecchelli R, et al. Differential roles for endothelial ICAM-1, ICAM-2, and VCAM-1 in shear-resistant T cell arrest, polarization, and directed crawling on blood-brain barrier endothelium. *J Immunol* 2010; 185: 4846–4855.
  33. Engen SA, Valen Rukke H, Becattini S, et al. The oral commensal *Streptococcus mitis* shows a mixed memory Th cell signature that is similar to and cross-reactive with *Streptococcus pneumoniae*. *PLoS One* 2014; 9: e104306.
  34. Sallusto F, Schaerli P, Loetscher P, et al. Rapid and coordinated switch in chemokine receptor expression during dendritic cell maturation. *Eur J Immunol* 1998; 28: 2760–2769.
  35. Enzmann G, Mysiorek C, Gorina R, et al. The neurovascular unit as a selective barrier to polymorphonuclear granulocyte (PMN) infiltration into the brain after ischemic injury. *Acta Neuropathol* 2013; 125: 395–412.
  36. Takeshita Y, Obermeier B, Cotleur A, et al. An in vitro blood-brain barrier model combining shear stress and endothelial cell/astrocyte co-culture. *J Neurosci Methods* 2014; 232: 165–172.
  37. Goncharova V and Khaldoyanidi SK. A novel three-dimensional flow chamber device to study chemokine-directed extravasation of cells circulating under physiological flow conditions. *J Vis Exp* 2013; 77: e50959.
  38. Xu H, Li Z, Yu Y, et al. A dynamic in vivo-like organotypic blood-brain barrier model to probe metastatic brain tumors. *Sci Rep* 2016; 6: 36670.
  39. Herland A, van der Meer AD, FitzGerald EA, et al. Distinct contributions of astrocytes and pericytes to neuroinflammation identified in a 3D human blood-brain barrier on a chip. *PLoS One* 2016; 11: e0150360.
  40. Neuhaus W, Lauer R, Oelzant S, et al. A novel flow based hollow-fiber blood-brain barrier in vitro model with immortalised cell line PBMEC/C1-2. *J Biotechnol* 2006; 125: 127–141.
  41. Cucullo L, Couraud PO, Weksler B, et al. Immortalized human brain endothelial cells and flow-based vascular modeling: a marriage of convenience for rational neurovascular studies. *J Cereb Blood Flow Metab* 2008; 28: 312–328.
  42. Erbeltinger N, Rapp F, Ktitareva S, et al. Measuring leukocyte adhesion to (primary) endothelial cells after photon and charged particle exposure with a dedicated laminar flow chamber. *Front Immunol* 2017; 8: 627.
  43. Mazzocchi AR, Man AJ, DesOrmeaux J-PS, et al. Porous membranes promote endothelial differentiation of adipose-derived stem cells and perivascular interactions. *Cell Mol Bioeng* 2014; 7: 369–378.
  44. Carter RN, Casillo SM, Mazzocchi AR, et al. Ultrathin transparent membranes for cellular barrier and co-culture models. *Biofabrication* 2017; 9: 015019.
  45. Chung HH, Casillo SM, Perry SJ, et al. Porous substrates promote endothelial migration at the expense of fibronectin fibrillogenesis. *ACS Biomater Sci Eng* 2018; 4: 222–230.
  46. Chung HH, Chan CK, Khire TS, et al. Highly permeable silicon membranes for shear free chemotaxis and rapid cell labeling. *Lab Chip* 2014; 14: 2456–2468.
  47. Johnson LM, Gao L, Shields IC, et al. Elastomeric microparticles for acoustic mediated bioseparations. *J Nanobiotechnology* 2013; 11: 22.



48. Bo L, Peterson JW, Mork S, et al. Distribution of immunoglobulin superfamily members ICAM-1, -2, -3, and the beta 2 integrin LFA-1 in multiple sclerosis lesions. *J Neuropathol Exp Neurol* 1996; 55: 1060–1072.
49. Drolez A, Vandehaute E, Julien S, et al. Selection of a relevant in vitro blood-brain barrier model to investigate pro-metastatic features of human breast cancer cell lines. *PLoS One* 2016; 11: e0151155.
50. Samuel W, Jaworski C, Postnikova OA, et al. Appropriately differentiated ARPE-19 cells regain phenotype and gene expression profiles similar to those of native RPE cells. *Mol Vis* 2017; 23: 60–89.
51. Hawkins BT and Davis TP. The blood-brain barrier/neurovascular unit in health and disease. *Pharmacol Rev* 2005; 57: 173–185.
52. Engelhardt B and Liebner S. Novel insights into the development and maintenance of the blood-brain barrier. *Cell Tissue Res* 2014; 355: 687–699.
53. Bhatia SN and Ingber DE. Microfluidic organs-on-chips. *Nat Biotechnol* 2014; 32: 760–772.
54. Walter FR, Valkai S, Kincses A, et al. A versatile lab-on-a-chip tool for modeling biological barriers. *Sensors and Actuators B: Chemical* 2016; 222: 1209–1219.
55. de Mesy Bentley KL, Trombetta R, Nishitani K, et al. Evidence of *Staphylococcus aureus* deformation, proliferation, and migration in canaliculi of live cortical bone in murine models of osteomyelitis. *J Bone Miner Res* 2017; 32: 985–990.
56. Kim E, Xiong H, Striemer CC, et al. A structure-permeability relationship of ultrathin nanoporous silicon membrane: a comparison with the nuclear envelope. *J Am Chem Soc* 2008; 130: 4230–4231.
57. Shulman Z, Shinder V, Klein E, et al. Lymphocyte crawling and transendothelial migration require chemokine triggering of high-affinity LFA-1 integrin. *Immunity* 2009; 30: 384–396.
58. Rudolph H, Klopstein A, Gruber I, et al. Postarrest stalling rather than crawling favors CD8(+) over CD4(+) T-cell migration across the blood-brain barrier under flow in vitro. *Eur J Immunol* 2016; 46: 2187–2203.